Toward a Self-Sensing Piezoresistive Pressure Sensor for all-SiC Monolithic Integration

Middelburg, Luke M.; van Zeijl, H.W.; Vollebregt, Sten; Morana, Bruno; Zhang, Guoqi

DOI
10.1109/JSEN.2020.2998915

Publication date
2020

Document Version
Final published version

Published in
IEEE Sensors Journal

Toward a Self-Sensing Piezoresistive Pressure Sensor for All-SiC Monolithic Integration

Luke M. Middelburg, H. W. van Zeijl, Sten Vollebregt, *Senior Member, IEEE*, Bruno Morana, and Guoqi Zhang, *Fellow, IEEE*

***Abstract*—This work focusses on the design and fabrication of surface micromachined pressure sensors, designed in a modular way for the integration with analog front-end read-out electronics. Polycrystalline 3C silicon carbide (SiC) was used to fabricate free-standing high topography cavities exploiting surface micromaching. The poly-SiC was in-situ doped and the membrane itself is used as piezoresistive element, thereby forming a so-called self-sensing membrane, easing fabrication. After sacrificial release, the cavity is sealed by conformal deposition of poly-SiC whereby the reference pressure of the absolute pressure sensor is determined. Aluminum and titanium metallizations were used and ohmic contacts were confirmed by wafer-scale measurements. Measurements were carried out on different devices ranging from 100 kPa down to 10 Pa at room temperature. The Wheatstone bridge yields a logarithmic response of 1.1 mVbar^{-1}V^{-1}. A square 300 μm device exhibits a logarithmic impedance behavior yielding a response of $\Delta R/R$ of 1.6×10^{-3}bar^{-1}. The realized pressure devices are a first step toward a SiC ASIC + MEMS platform for intended operation in harsh environments, such as industrial process monitoring, combustion control or structural health monitoring. The future outlook of the integration concept implies extended functionality by front-end transducer read-out, signal amplification and communication.**

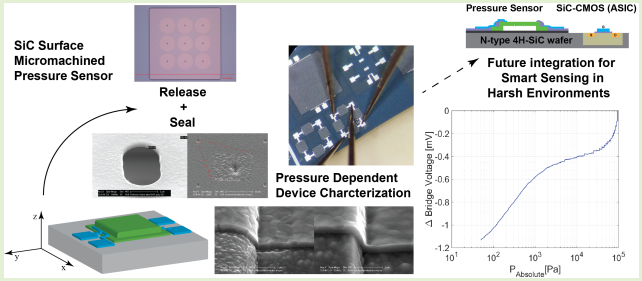

***Index Terms*— Silicon carbide, absolute pressure sensor, MEMS, surface micromaching.**

I. Introduction

SILICON carbide is a compound semiconductor with a larger bandgap compared to silicon, resulting in unique physical properties. A higher critical electrical field strength and a larger thermal conductance compared to silicon has resulted in the adoption of silicon carbide in power electronics. In addition, thanks to its larger bandgap, and inherent lower intrinsic carrier concentration at elevated temperatures, silicon carbide active devices such as BJTs and MOSFETs in 4H- or 6H-SiC keep showing the desired electronic behavior, even beyond 500 °C [1], [2]. As a result SiC CMOS technologies exploiting mono-crystalline SiC (such as 4H or 6H) are promising for the development of low-voltage front-end read-out electronics.

Manuscript received May 26, 2020; accepted May 28, 2020. Date of publication June 1, 2020; date of current version September 3, 2020. This work was supported in part by the European Project IoSense: Flexible FE/BE Sensor Pilot Line for the Internet of Everything, in part by the Electronic Component Systems for European Leadership Joint Undertaking under Grant 692480, and in part by the European Union's Horizon 2020 Research and Innovation Programme in Germany, Saxony, Austria, Belgium, The Netherlands, Slovakia, and Spain. The associate editor coordinating the review of this article and approving it for publication was Dr. Carlos Marques. *(Corresponding author: Luke M. Middelburg.)*

The authors are with the Department of Microelectronics, Delft University of Technology, 2628 CD Delft, The Netherlands (e-mail: l.m.middelburg@tudelft.nl).

Digital Object Identifier 10.1109/JSEN.2020.2998915

In recent years, research has been conducted into the application of silicon carbide for the fabrication of sensors, mainly intended for harsh environments. Properties such as a high Young's modulus, high acoustic velocity, high radiation hardness, high chemical intertness and the high melting point make SiC an interesting candidate for many different sensors. Wright *et al.* give an overview of different SiC based sensors, ranging from gyroscopes and gas sensors to pressure sensors, along with specific harsh environment applications, such as combustion control and space applications [3]. Senesky *et al.* discuss the application of SiC sensing structures and electronics specifically for health and performance monitoring in aerospace systems [4].

Pressure sensors are present in numerous applications, which makes them an ideal candidate to consider for monolithic integration with state-of-the-art SiC CMOS processes. Pressure sensors intended for harsh environments can for example be used for combustion monitoring to improve efficiency and reduce emissions of unwanted combustion products [2]. Additionally, they can be used to monitor pressures in geothermal wells and turbines [5], [6]. A pressure sensor which can be fabricated in such a modular way that it can be incorporated in the back-end-of-line (BEOL) part of a CMOS process, would enable a platform on which the physical pressure transducer is monolithically integrated with the front-end CMOS read-out electronics. From a measurement system's

perspective, it is highly desirable to have the read-out electronics, for example impedance read-out or signal amplification, as close as possible to the physical transducer, in order to minimize noise contributions originating from interconnect, EMI, or parasitic impedances. Another advantage of the integrated electronics is that the the read-out is performed directly in the electrical domain. Examples exist in literature where the read-out of membrane deflection is done using optical fibers [7]. Moreover, because of the inertness of silicon carbide, the usage of both a SiC sensing structure and SiC CMOS electronics relaxes the requirements on the packaging of bare dies.

Numerous pressure sensors have been reported in literature featuring silicon carbide, both exploiting thin-film carbide (typically 3C polytype based) and bulk substrates (typically 4H polytype based). Hoogerwerf *et al.* reports on a mono-crystalline 4H-SiC based pressure sensor using a sealed reference cavity [8]. Despite the structure being fully crystalline silicon carbide based, the proposed design relies on DRIE etching of crystalline SiC in combination with wafer bonding and is less suited for integration with SiC CMOS. Moreover results such an implementation in double the substrate costs.

A pressure sensor formed by laser scribing bulk 4H-SiC was reported by Nguyen *et al.* [9] resulting in a rather large required membrane area of 5 x 5 mm^2, due to the rough surface finish of such an ablation method. Although the electrical and mechanical properties of the crystalline SiC are fully exploited, the design relies on die-bonding with epoxy to a chip carrier in order to form an absolute pressure sensor. Also, from a miniaturization perspective, a membrane formed by laser scribing is undesirable, especially taking into account the high area cost of a SiC CMOS wafer.

Research into the piezo resistive properties of in-situ doped polycrystalline 3C-SiC was recently published by Phan *et al.* [10] and it was reported that gauge factors (GFs) up to -10 can be achieved [11], comparing to 20.8 for crystalline 4H-SiC [12]. Although the gauge factors which can be obtained by the usage of polycrystalline in-situ doped 3C-SiC are significantly lower compared to the mono-crystalline counterparts, the usage of polycrystalline has significant advantages, especially in the context of monolithic integration with SiC CMOS. Bulk micromachining of crystalline SiC can be performed, but is not trivial since it requires metal masking layers when depths exceeding several μm's need to be etched, due to the otherwise poor selectivity [12]–[16]. The significant research interest in SiC and other wide bandgap materials is illustrated by a novel opto-electronic coupling mechanism that was recently reported by Nguyen *et al.* [17], [18]. This coupling mechanism is used to boost the gauge factor by using illumination of SiC, thereby generating a gradient of charge carriers. The same effect is exploited by Li *et al.* in the application of 3C-SiC nanowires which are illuminated with UV-light to enhance piezoresistive behavior [19]. These works illustrate the importance of further investigation of novel concepts of piezoresistive materials and sensors.

Using thin-film polycrystalline 3C-SiC omits the need for the rather complex bulk micromachining. Moreover, the process flow can be designed such that it fits in the back-end processing of a SiC CMOS technology, and that the sensor can be fabricated on different types of substrates, enabling prototyping on well-available and cheaper silicon substrates. In the latter case, the influence on the mechanical design of the different coefficients of thermal expansion (CTEs) need to be taken into account. Surface micromachining thin-films results in a higher degree of design flexibility, since membrane dimensions can be chosen freely regardless of the substrate thickness. Moreover, because the formation of an absolute pressure sensor based on a reference pressure inside a sealed cavity is more easily achieved in a surface micro machined, thin-film based solution.

Capacitive surface micro machined pressure sensors exploiting poly-SiC are reported in literature. Beker *et al.* realized a surface micro machined capacitive pressure sensor featuring a cavity with a reference pressure from polycrystalline SiC. However, operation up to only 180 °C was demonstrated [5]. Chen and Mehgregany have realized a capacitive surface micromachined pressure sensor showing operation up to 574 °C for in-cylinder measurements [20]. The disadvantage of specifically capacitive surface micromachined pressure sensors is that a second electrode is needed for the actual capacitor, requiring additional processing steps in the back-end module and hindering integration ability with SiC CMOS. Piezo resistive pressure sensors using poly 3C-SiC have been fabricated by Chien-Hung *et al.* [21], but the design proposed relies on bulk etching of silicon substrates, which is undesired for the scope of this work.

Phan *et al.* used thin-film SiC for the fabrication of a suspended membrane of only 200 nm, forming a pressure sensor [22]. The layer was interfaced using nickel electrodes and its n-type doping concentration was 1×10^{16} cm. A unique property of this device was that no separate piezo resistors were designed to transduce the stress in the membrane to the electrical domain. Although the device described in this work was fabricated on silicon substrates and relies on bulk etching of this substrate, the concept of a self-sensing membrane eases fabrication significantly, since it reduces the number of processing steps. This concept will be applied in this work to a pressure sensor which is fully surface micro machined, omitting the need for bulk etching and while maintaining the advantages of using poly-SiC.

Therefore, the goal of this paper is to develop a modular pressure sensor that can be integrated monolithically with SiC CMOS based on 4H-SiC substrates, as schematically illustrated by Fig. 1. This means that the fabrication of the device must fit inside the back-end fabrication of a SiC CMOS technology, implying challenges regarding thermal budget, contamination and metallization. In order to comply with this goal, this work will focus on the usage of intrinsic and in-situ doped n-type polycrystalline thin-film 3C-SiC. Besides, the concept of a self-sensing membrane will be investigated. The high degree of modularity is a third important starting point of the design. By varying the membrane thickness, shape,

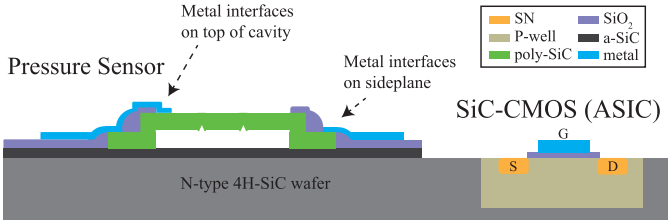

Fig. 1. A conceptual representation of the possible monolithic integration of the designed MEMS pressure sensor with SiC-CMOS.

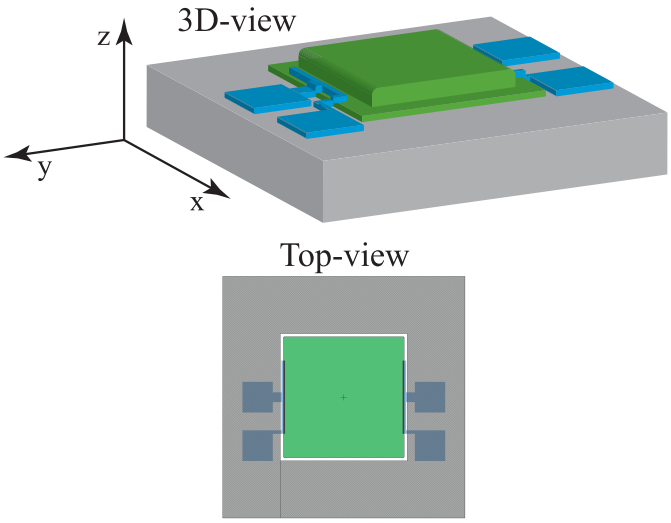

Fig. 2. A schematic drawing of the design of the pressure sensor.

length, width and the dopant concentration of the membrane layer freely, the device can be tailored to specific device performance related to different applications.

II. Design

The design is based on a surface micromachined sealed cavity created by a suspended membrane made of polycrystalline 3C-SiC layers. These SiC layers are deposited by low pressure chemical vapor deposition (LPCVD). The cavity holds a reference pressure inside which is created during the sealing process of the released membrane and after the removal of the sacrificial layer. The membrane consists of a stack of an intrinsic poly-SiC layer and a piezo resistive in-situ n-type doped poly-SiC layer. The piezo resistive layer will directly be used to transduce the pressure-induced strain of the membrane into a resistance variation. Electrodes will be patterned directly on top of the cavity, enabling four point resistance measurements. A schematic drawing of the proposed design is displayed in Fig. 2.

A. Analytical Device Modeling

The design of the device is bounded by cleanroom fabrication feasibility aspects, such as the maximum poly-SiC layer thickness of 5 µm due to the deposition process. The theory of Meleschenko [23] can be used to link a uniform pressure on a square membrane to the maximum deflection (typically in the center in the case of a square membrane), as described by equation (1).

$$P = E\frac{h^4}{a^4}[g_1\frac{w_0}{h} + g_2(\frac{w_0}{h})^3] \tag{1}$$

TABLE I
Design Parameters

Symbol	Quantity	Value
E	Young's modulus	430 GPa [26]
ν	Poisson ratio	0.168
w_0/h	Linearity constraint	0.2
2a	Membrane width	300 µm
h	Membrane thickness	2.7 µm
σ_c	Critical stress	3.16 GPa [27]
ρ	Density LPCVD SiC	3.18 kg m^{-3} [1]

In which, P is the pressure in [Pa], E the Young's modulus, h the thickness of the membrane in [m], a half of the width ($2a$ = membrane width), w_0 the maximum deflection of the membrane in [m], and g_1 and g_2 are constants that include the Poisson ratio ν. Using 0.168 for the Poisson ratio of poly-SiC, g_1 and g_2 can be determined:

$$g_1 = \frac{4.13}{(1-\nu^2)} = 4.25 \tag{2}$$

$$g_2 = \frac{1.98(1-0.585\nu)}{(1-\nu)} = 2.15 \tag{3}$$

Using equation (1), it can be seen that the pressure is linearly linked to the maximum deflection w_0 as long as the first term within the square brackets is much smaller than the second term, which is the third power of the ratio between the maximum deflection and thickness of the membrane. As reported in literature [24], [25], to satisfy this condition typically a value of 0.2 is employed for the w_0/h ratio. This would allow the second term to be only 4% of the first term, thus ensuring a linear dependence between the pressure and the maximum deflection. In this case the maximum deflection would be equivalent to 20% of the membrane thickness at most. Using equation (1) for a membrane thickness of 2.7 µm and a membrane width of $2a$ = 300 µm results in a maximum pressure for linear deflection of 39.14 kPa with a corresponding deflection of 540 nm. The maximum stress which occurs at the center of the edge of a square membrane (x= +/−a) is given by equation (4). Based on this equation, the maximum pressure for linear deflection results in a maximum stress of 1.21×10^8 N m^{-2}. When a pressure of 100 kPa is considered, the maximum stress by equation (4) is 3.08×10^8 N m^{-2}.

$$\sigma_{max} = P(\frac{a}{h})^2 \tag{4}$$

In harsh environments, a relevant parameter is the pressure beyond which yielding starts to occur, also called burst pressure, which is determined by the critical stress σ_c and given by equation (5).

$$P_B = \frac{\sigma_c}{(\frac{a}{h})^2} \tag{5}$$

By substituting the design parameters as summarized in Table I in equation (5), a burst pressure of 1.02 MPa is obtained. This in the case of a free standing membrane where the deflection is not limited by the cavity height. The resonance frequency of the membrane should be considered for applications where the dynamic behavior is of importance.

TABLE II
SIMULATION PARAMETERS

Quantity	Value
Membrane width	300 µm
Membrane thickness	2.7 µm
Contact thickness	1 µm
Contact length	180 µm
Contact width	2 µm
Reference pressure	20 Pa
Piezoresistive coupling coefficient	-2.33×10^{-11} Pa^{-1}
Residual stress	487 MPa

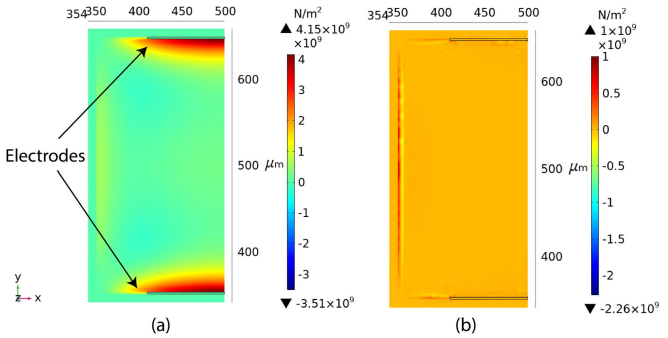

Fig. 3. (a) The stress tensor in y-direction at 100 kPa; (b) The stress tensor in z-direction at 100 kPa.

This frequency can be expected to be high, thanks to the high stiffness of the used polycrystalline SiC material and the relatively low mass of the membrane itself. The resonance frequency is given by equation (6).

$$f_r = 1.65 \frac{h}{a^2} \sqrt{\frac{E(1-\nu^2)}{\rho}} \tag{6}$$

which gives a resonance frequency of 79 MHz.

B. Finite Element Modeling

Based on the proposed design, finite element analysis (FEA) was performed using COMSOL. The poly-3C-SiC material was defined from a blank material. The piezoresistive coupling matrix relates the mechanical stress σ to a change in resistivity $\frac{\Delta\rho}{\rho}$ as expressed by equation (7) [10]. Note that for a polycrystalline material, as used in this work, the piezoresistive coupling matrix can be simplified to a scalar, since the piezoresistive properties are not dependent on the directions of the crystal, resulting is an isotropic piezoresistive coupling coefficient.

$$\frac{\Delta\rho}{\rho} = \pi\sigma \tag{7}$$

The gauge factor is linked to the piezo resistive coupling value via the Young's Modulus as described by equation (8).

$$GF = E\pi \tag{8}$$

In which E is the Young's modulus. From literature it can be concluded that the highest gauge factors are obtained for a target bulk resistivity of polycrystalline 3C-SiC of approximately 0.1 Ωcm [10], [11]. Considering a gauge factor of −10, a piezo resistive coupling value of -2.33×10^{-11} Pa^{-1} is obtained. COMSOL expects a piezo resistive coupling value which is multiplied with the bulk resistivity. The piezoresistive coupling coefficient equals then -2.33E-14 Ωm/Pa, which equals -2.33×10^{-14} m^4 s^{-1} A in SI-units. The cavity will be sealed at 80 Pa and 860 °C. Applying gas laws of Gay-Lussac and under the assumption of constant volume, a value of about 20 Pa is obtained when the cavity is at 25 °C. Other simulation parameters used are reported in Table II.

Although the geometry can be varied freely within the process boundary conditions, a square membrane with a side length of 300 µm with a thickness of 2.7 µm was modeled. Because the membrane itself is used as piezo resistive sensing element, the dimensions and positioning of the electrodes is largely influencing the sensitivity of the device. The length of the electrodes was designed such that they align with the regions of maximum stress. Two design options are considered, one where the electrodes are deposited directly on top of the membrane and one where the electrode is formed on the 'sideplane', right next to the cavity. For sensitivity reasons, the first option is highly preferred, but requires the metal to be deposited over one additional flank. Both design options are illustrated in Fig. 1, the electrode on top of the cavity and on the side plane on the left and right side respectively. In the simulation, the electrodes positioned directly on top of the cavity are considered. A line of symmetry was added to reduce computational load. Aluminum was chosen as material for the electrodes, while the membrane itself is based on the poly-SiC.

The reference pressure inside the cavity was modeled by applying a boundary load on the bottom of the membrane, while the simulated pressure was applied by a boundary load on the outside of the cavity, thereby yielding a pressure difference. Fixed constraints were used to bound the device as if it would be processed on a wafer. Additionally, a boundary load was applied to the membrane to account for the residual stress in the poly-SiC which was characterized during fabrication (Section III). A parametric sweep was used to investigate the membrane response in which the pressure was swept from 10 Pa to 100 kPa. The y- and z-components of the stress tensor at the maximum pressure of 100 kPa is included in Fig. 3, from which it can be seen that the electrodes match the regions of maximum stress. As expected, due to the uniformly applied pressure and to the small thickness of the layer the stress in the z-direction is uniform.

The simulated displacement in the minus z-direction with an applied pressure of 100 kPa equals 1.2 µm whereas the simulated deflection at 39.15 kPa (that is the maximum pressure for linear deflection) equals 540 nm, which is equal to the analytical derivation. The piezoresistive multi-physics module was used to study the piezoresistive response of the membrane.

$\frac{\Delta R}{R}$ was determined by using the base resistance at zero pressure difference (P = 20 Pa) and plotted against the swept pressure using a logarithmic x-axis, as shown in Fig. 4. The simulations reveal that $\frac{\Delta R}{R}$ is a logarithmic function of pressure from approximately 30 kPa. When the gauge factor is calculated back based on the derived volumetric strain, the gauge factor of -10 is obtained, verifying the simulation.

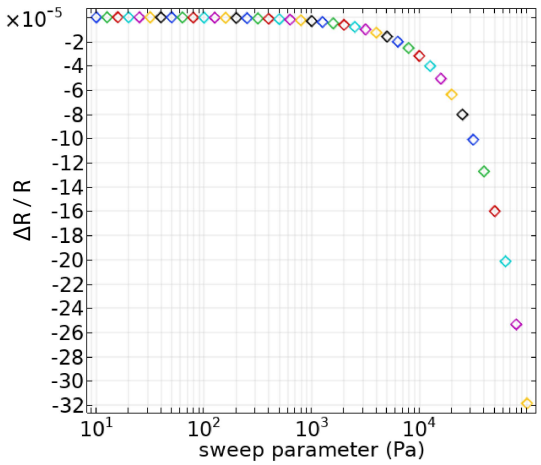

Fig. 4. $\frac{\Delta R}{R}$ as function of the swept pressure to investigate the piezo resistive behavior.

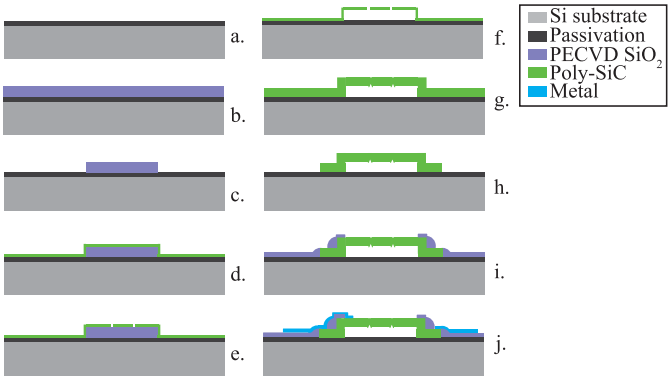

Fig. 5. The process flow used during fabrication.

III. Fabrication

A schematic illustration of the process flow is reported in Fig. 5. A layer of low-stress amorphous SiC with a thickness of 720 nm was deposited by plasma enhanced chemical vapor deposition (PECVD), this served to electrically isolate the device from the silicon substrate (Fig. 5a). Furthermore functions this layer as etch barrier during the sacrificial etch. The bulk electrical resistance of the amorphous SiC layer is in the order of MΩcm. Subsequently, a layer of 2.5 µm SiO_2 was deposited by PECVD from which the mesa structures will be formed (Fig. 5b). By using a photoresist (PR) layer of 4.0 µm lithography of the mesa structures was performed, subsequently they were etched by using a standard SiO_2 plasma etch recipe in a RIE etchter (Fig. 5c).

After the mesas have been patterned, the first intrinsic poly-SiC layer of 700 nm was deposited by LPCVD. Dichlorosilane (SiH_2Cl_2) and acetylene (C_2H_2) were used as precursor gasses with flow rates of 123 sccm and 18.85 sccm, respectively in a hot-wall LPCVD furnace operating at a deposition temperature of 860 °C (Fig. 5d). More information on the poly-SiC recipe used is given by Morana *et al.* [28]. With a four probe Kelvin sheet resistance measurement tool, the bulk resistivity of the intrinsic SiC layer was measured to be 439.8 Ωcm. Characterizations of the doped piezoresistive poly-SiC layer performed by using high resolution scanning

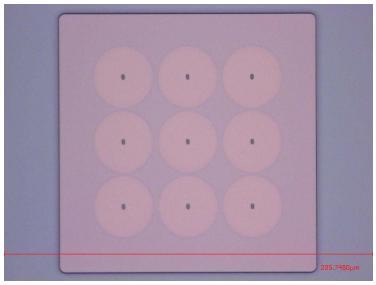

Fig. 6. A microscopy image from top view of the membranes after initial sacrificial etching of the SiO_2. The circular areas indicate where the sacrificial oxide has been etched away. Longer etching is required to fully release the membranes.

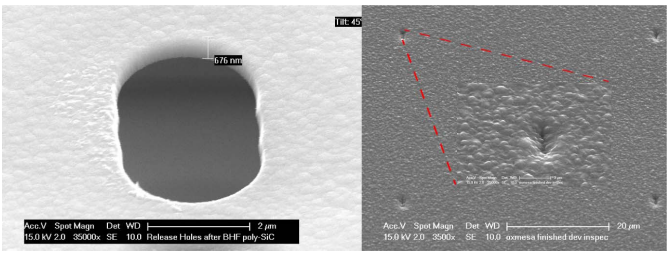

Fig. 7. SEM images of the release hole: After sacrificial etch (left) and after sealing (right).

electron microscope and atomic force microscopy revealed a grain size of 145±7 nm. Due to the high topography of the patterned structures, MicroChemicals 12XT-20PL10 chemically amplified PR was used to cover the entire cavities. A PR thickness was achieved of 7 µm by manual spincoating. The release holes are oval shaped and have a width of 2 µm and a length of 4 µm, the shape can be tuned by exposing the image with circular release holes multiple times with lateral offset steps. It is important that the width is maximum half the target thickness of the second SiC deposition in order to ensure sealing of the cavities. The release holes were etched in the instrinsic poly-SiC using a customly developed plasma etch recipe based on SF_6 and O_2 and performed at 0 °C in a DRIE etcher (Fig. 5e). The sacrificial SiO_2 was etched by using vapor HF, the removal was step-wise monitored by optical microscope inspections. This was possible thanks to the optical transparency of the poly-SiC layer. This is shown in Fig. 6 where circular shapes centered at release holes are clearly visible. These indicate the removal of the SiO_2 (Fig. 5f).

A scanning electron microscope (SEM) image of the release hole after sacrificial etch is shown in Fig. 7 (left). After the sacrificial oxide was completely etched, the second poly-SiC layer of 2 µm was deposited (Fig. 5g). For this deposition, ammonia (NH_3) was added during the deposition as n-type dopant. This recipe used 80 sccm dichlorosilane (SiH_2Cl_2), 16 sccm and acetylene (C_2H_2) and 1.5 sccm ammonia, targeting a bulk resistivity of 0.02Ωcm. Although this value is lower than that employed in the simulation and selected for maximizing the gauge factor, this recipe was chosen to make sure that ohmic contact are formed. In general, moderate tensile stress is desired for the realization of flat, non-buckled membranes. The residual stress of the poly-SiC:N layer was determined by wafer curvature measurements performed using

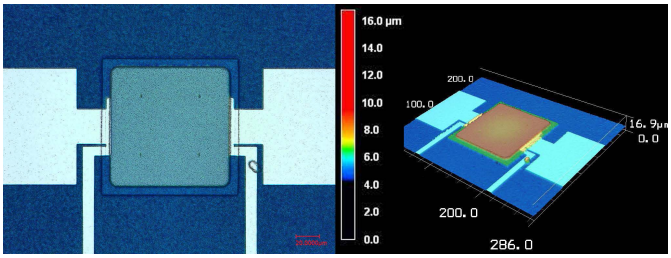

Fig. 8. An optical microscope picture (left) and a height map (right) of a finalized 100μm device.

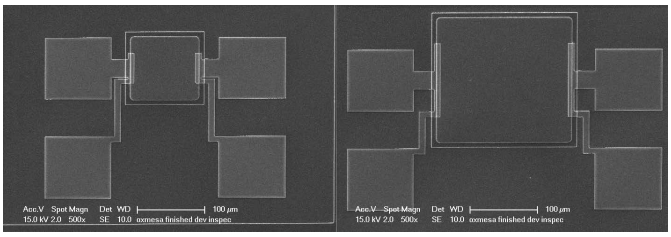

Fig. 9. SEM images of the 100μm and 200μm square cavities.

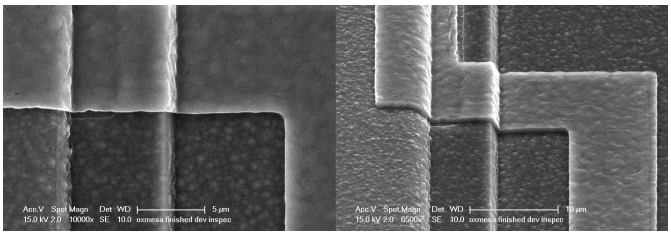

Fig. 10. SEM images of the step coverage of the metal to cavity contact; without tilt (left), with a tilt of 45° (right).

a Flexus 2320S and by means of Stoney's formula, this resulted in a tensile stress with a magnitude of 487 MPa.

After the poly-SiC:N deposition, the total stack of 2.7 µm consisting of the intrinsic and doped poly-SiC layer around the cavities was etched, while landing in the isolating passivation layer. In order to minimize the area where parasitic currents through the intrinsic poly-SiC could occur, the 700 nm thick intrinsic poly-SiC layer was etched away, while landing on the isolating amorphous SiC. After patterning, the poly-SiC stack was etched using the same procedure as was used to etch the release holes (Fig. 5h). To isolate and passivate the functional poly-SiC layer, a layer of SiO_2 of 500 nm was deposited on the wafers. This SiO_2 was etched at the locations of the electrodes and on top of the membrane. Otherwise, the SiO_2 layer would affect the mechanical properties of the poly-SiC stack (Fig. 5i). In order to form the electrodes, metal traces and probe pads, 1000 nm of AlSi(1%) was sputtered at 350 °C. The AlSi(1%) was etched using a chlorine based recipe in an inductively coupled plasma (ICP) metal etcher (Fig. 5j).

The completed devices were inspected by a SEM and a Keyence VK-X250 3D laser scanning confocal microscope. Fig. 8 shows an image of the optical inspection (left) with the height map (right), where the deflection towards the substrate by the atmospheric overpressure can be noticed. SEM images of the complete devices are included in Fig. 9. The continuity of the metal traces over the step heights was inspected as indicated in Fig. 10.

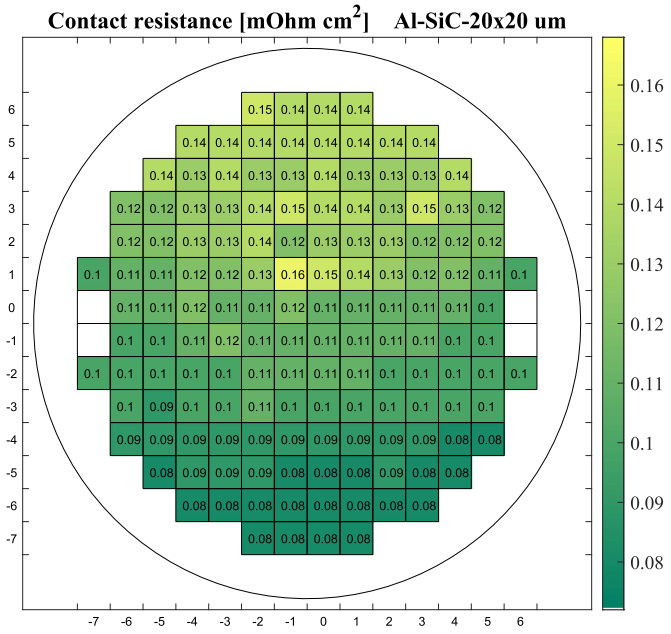

Fig. 11. Wafer scale measurements of specific contact resistances for the 20 × 20μm Kelvin cross bridges with Al metallization.

IV. Results and Discussion

After fabrication, the wafers were diced and the pressure devices were characterized. Additional test wafers were fabricated with electronic test structures. These were used to characterize ohmic contacts by measuring Kelvin cross bridges (KCBs).

A. Ohmic Contacts

KCBs with two different sizes are measured on wafer scale to verify if the metal-to-poly-SiC contacts exhibit an ohmic behavior and to quantify the specific contact resistance ρ_c. In the KCB, a square contact with a specific area between a strip of poly-SiC and metal is made. A known voltage is forced between one SiC/metal pair, whereas the voltage drop over the other pair is measured. The specific contact resistance is subsequently determined based on the area of the measured contact hole, the measured current through the force pair and the voltage on the sensing pair. In addition to the sputtered AlSi(1%), also Ti was characterized, because this metal would enable measurements carried out at temperature beyond the melting point of aluminum, i.e measurements beyond 575 °C. The KCBs were characterized by a four point Kelvin measurement where a voltage is forced ranging from −2 V to 2 V, while the differential voltage of the other two pads is measured. The 20 x 20 µm KCB structures were measured at wafer scale, the result is shown in Fig. 11. What can be seen from the color wafermap is that a gradient appears to be present from the bottom to the top of the wafer, where ρ_c varies from 1×10^{-4} Ωcm^2 to 2.1×10^{-4} Ωcm^2. It can be concluded from the linearity of the fitted IV curve as displayed in Fig. 12 that the contact is highly ohmic for the employed bias and temperature conditions.

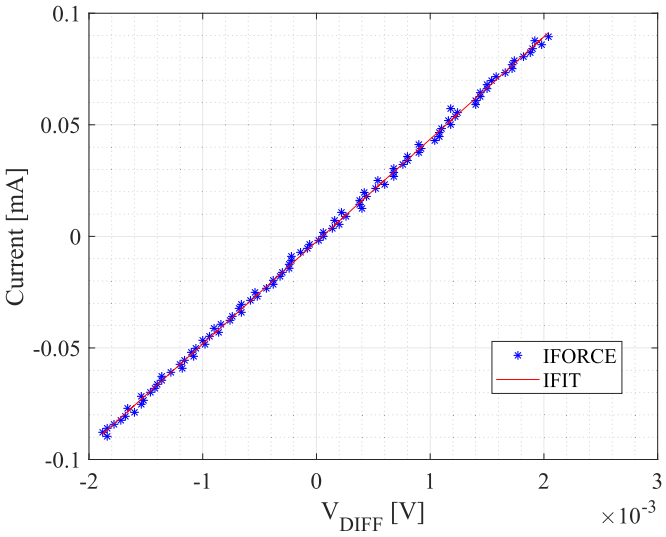

Fig. 12. The IV-curve for the maximum contact resistance (die −2, −7).

The mean value and standard deviation of the specific contact resistances measured for the AlSi(1%) and Ti sputtered at 350 °C equal $\mu = 0.129$ mΩcm^2, $\sigma = 0.0369$ mΩcm^2 and $\mu = 0.149$ mΩcm^2, $\sigma = 0.0307$ mΩcm^2 respectively. Overall, it can be concluded from these measurements that the as-deposited AlSi(1%) and Ti metallizations yield to negligible contact resistances compared to the resistance of the pressure devices. For the square-shaped membrane with 300 µm side length, the contact resistance (based on the design and characterized ρ_c) equals 5.33Ω which is about 3.5% of the membrane resistance of 153Ω and thus negligible.

B. Pressure Measurements

The pressure setup consists of a Nextron MPS-CHH microprobe chamber with a ceramic chuck. This chamber can be pumped down, while electrical measurements can be carried out using four available probe needles with a 20 µm rhodium coated tip. The vacuum is arranged via a BocEdwards XDS-10 scroll pump connected to a Bronkhorst EL-PRESS pressure controller. This controls the pressure inside the chamber by adjusting the flow. The pressure controller houses a reference pressure sensor and is controlled using a personal computer (PC). The resistance of the pressure devices under test is measured using a Keithley 2612B source measurement unit (SMU) enabling a four probe Kelvin measurement. A schematic overview of the measurement setup is shown in Fig. 13.

1) Single Device: Initially the square-shaped membrane with 300 µm side length was measured. The membrane was biased with a constant voltage of 1 V, while the current over the force pair and the voltage over the sensing pair were measured using the SMU. Simultaneously, the microprobe station was pumped down from atmospheric pressure down to 10 Pa. The resistance- and pressure was measured using a sample rate of 1 sample/s and the entire measurement lasted for 131 s.

$\frac{\Delta R}{R}$ was determined by using the membrane resistance at 100 kPa as base resistance R and with $\Delta R = R_{measured} - R$. Fig. 14 shows $\frac{\Delta R}{R}$ against absolute chamber pressure.

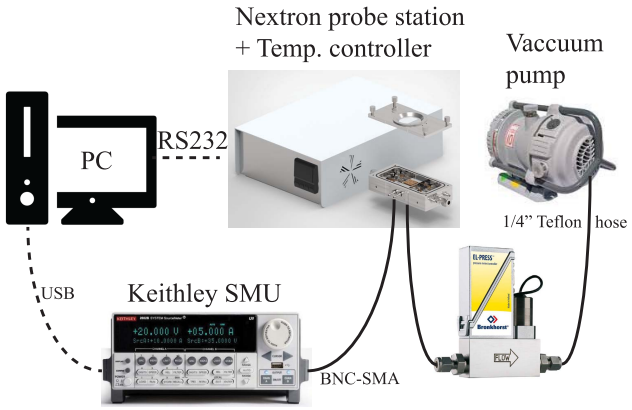

Fig. 13. A schematic overview of the pressure measurement setup.

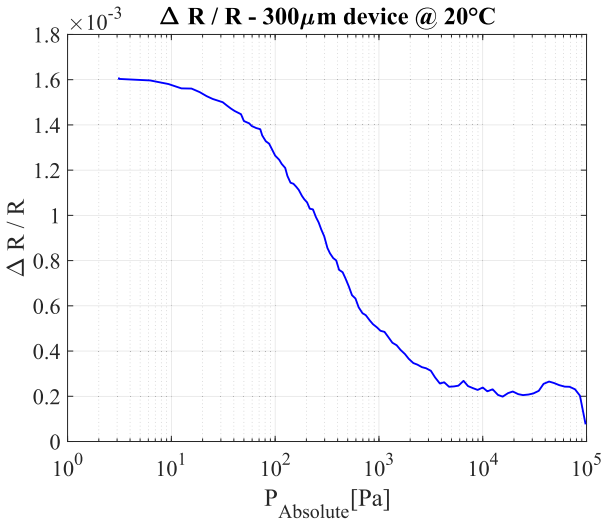

Fig. 14. $\frac{\Delta R}{R}$ versus pressure in semi-logarithmic scale for the measured single square membrane of 300µm. The base resistance was taken at the start of the pump down at 100 kPa.

Due to the high pump speed at the start of the pumpdown in this measurement, the result is noisy between 1×10^4 Pa and 1×10^5 Pa. Based on this result it can be seen that the response starts to become unambiguous from 1×10^4 Pa and below, whereas the most sensitive region is between 1×10^2 Pa and 1×10^3 Pa, where the resistance response is logarithmic. The resistance vs. pressure behavior can be explained by the decreasing absolute pressure in the microprobe station, resulting in a smaller pressure difference ($P_{ref} \approx 20$ Pa). As a result of the reduced pressure difference, the strain and thus stress on the membrane is reduced. The measured increase in resistance of the membrane while reducing the strain on the membrane is in agreement with reported negative gauge factors for poly-SiC [10], [11].

The logarithmic behavior of $\frac{\Delta R}{R}$ as function of pressure sensor resembles the simulated behavior as included in Fig. 4, although the result shows that the measurement range of the realized device is shifted to smaller pressures. The measured $\frac{\Delta R}{R}$ of -1.6×10^{-3} bar^{-1} (decreasing resistance with increasing absolute pressure) is different from the value as simulated in Sec. II-B of -3.23×10^{-4} bar^{-1}. In order to investigate

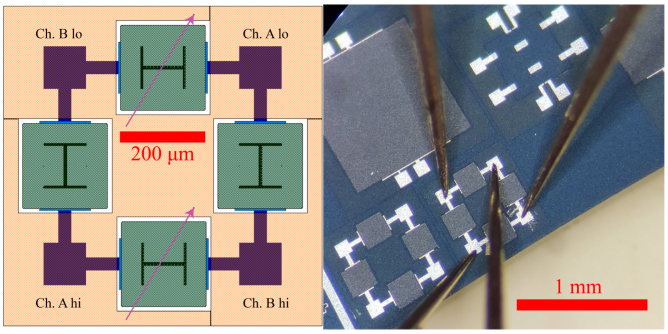

Fig. 15. The Wheatstone bridges connections to the SMU; schematically (left) and through microscope (right).

this discrepancy, the gauge factor can be determined based on the measured $\frac{\Delta R}{R}$ by using the following equation:

$$\mathrm{GF} = \frac{\frac{\Delta R}{R}}{\epsilon} \tag{9}$$

In which ϵ equals the strain, which is determined using the volumetric strain as available from our numerical model yielding to 1.64×10^{-5}. Using equation 9 with a measured $\frac{\Delta R}{R}$ of $-1.6 \times 10^{-3}\,\mathrm{bar}^{-1}$ results in a calculated gauge factor of -91. This value is much higher than reported gauge factors in literature for poly 3C-SiC. Eickhoff *et al.* [11] reports for example a GF of -10 for n-type doped poly 3C-SiC, whereas Yasui *et al.* [29] reports a GF of -2.1 for such a layer. In addition, Strass *et al.* [30] reports a GF of -5 for randomly nitrogen-doped poly-SiC. Although the derived value of -91 for the gauge factor is unrealistically high compared to literature, it suggests that the gauge factor used in the simulation is higher in reality. The simulation was furthermore based on the Young's Modulus and Poisson ratio as reported in literature. The actual values of these two properties might differ, which can be another reason for the discrepancy between the simulated and measured sensitivities.

2) Wheatstone Bridge: The Wheatstone half-bridge consisting of two non-released and two released square membranes having a side length of 200 µm was measured. The individual pressure devices of the Wheatstone bridge feature 7 µm wide electrodes through 5 µm contact holes on the sideplane of the membrane. The purpose of the non-released membranes is to function as dummy devices which experience identical circumstances as the sensing membranes. The bridge was biased using a constant voltage of 1 V, while the bridge voltage was measured using the two other probe needles at the sensing pads. In order to read out the Wheatstone bridge, a dual channel configuration was set for the SMU. Channel A was used to deliver a constant voltage, while channel B was used to continuously measure the bridge voltage as indicated in Fig. 15. In a similar way as for the characterization of the single device, the bridge voltage was continuously measured while pumping down the probe station. Data were acquired with a sample rate of 1 sample/s and the entire measurement lasted for 249 s.

The offset voltage present at 100 kPa and corresponding to 617.9 mV was subtracted from the measured bridge voltage,

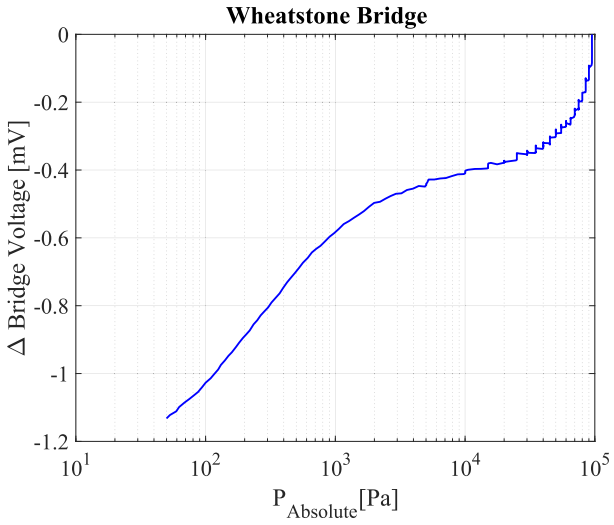

Fig. 16. The bridge voltage as function of pressure after an offset voltage correction at 100 kPa.

resulting in the Δ bridge voltage against pressure as shown in Fig. 16. As can be seen from this results, the bridge voltage is decreasing with decreasing pressure when pumping down from atmospheric pressure. This can be explained by the operation of the Wheatstone bridge; at $t = 0$ two out of four pressure devices experience a large overpressure and the bridge is essentially out of balance. As time passes the absolute pressure is decreasing and thus the pressure difference is decreasing. The resistance of the released device is getting closer to the resistance of the non-released devices and the bridge becomes more balanced. In the data analysis, the absolute value of the bridge voltage was plotted for convenience. The maximum bridge voltage difference at 50 Pa equals 1.1 mV. In the pressure range from 100 kPa down to 2000 kPa, the bridge voltage difference shows a linear response, which is followed by a straight line in between 50 Pa and 1 kPa, which shows that the bridge voltage is a logarithmic function of the pressure. The difference in measurement range between the single device and the Wheatstone bridge can be explained by the different geometry of the (individual) devices. The Wheatstone bridge consists of four square membranes having a side length of 200 µm, while for the single device the side length is 300 µm. The measurement range of the smaller devices is shifted to larger pressures, as is indicated by the absence of saturation in the measurement result of the Wheatstone bridge. To give an indication of the stability of the bridge voltage, a temperature sweep was performed at constant (atmospheric) pressure, resulting in a deviation of 0.19 mV when the temperature is varied from 25°C ro 125°C.

V. Conclusion

Surface micromachined absolute pressure sensors have been designed and realized based on the self-sensing concept enhancing device and processing flexibility to make integration with SiC CMOS possible. Intrinsic and in-situ doped polycrystalline SiC was used as functional material and its bulk resistivity and residual stress were measured. Finite element modeling was applied to verify the desired mechanical and

piezo resistive behavior and the results were in agreement with the analytical modeling. Ohmic behavior of the contacts between lowly doped poly-SiC and Ti and AlSi(1%) was verified by measuring test structures.

A single pressure device with a side length of 300 µm was measured and a logarithmic response for $\frac{\Delta R}{R}$ was obtained yielding a full range response of $-1.6 \times 10^{-3}\,\text{bar}^{-1}$, where the sensitivity is maximum between 1×10^2 Pa and 1×10^3 Pa. The reported negative gauge factors were confirmed by the measurements and the response is larger than the simulated value. Despite a shift in measurement range, the simulated logarithmic behavior of the devices is in agreement with the pressure measurements performed. A Wheatstone half-bridge was measured and the difference in bridge voltage over the full range resulted 1.1 mV. Upon decreasing the applied pressure and starting from 100 kPa it is shown that the bridge voltage difference has a linear response down to 2000 Pa while it exhibits a logarithmic trend below this pressure.

It can be concluded that the concept of a self-sensing membrane is successful and can be used to realize surface micromachined pressure sensors, of which the functional material is solely polycrystalline SiC. The self-sensing concept enables omission of discrete piezoresistors on a membrane or a buried electrode when a capacitive pressure sensor is considered. The device geometry would allow tailoring the geometry to match the performance with different applications. The convenient processing is beneficial for future integration with SiC CMOS, for example for impedance read-out, analog to digital conversion or signal amplification.

Future work involves investigation of high temperature performance and hysteresis effects. Stability of the devices and ohmic contacts for extended periods of time at high temperatures and in harsh environments is also considered as future work.

Acknowledgment

J. Romijn is acknowledged for this assistance during the wafer scale measurements. Additionally, the authors would like to thank J. Mo for his contribution in characterizing different poly-SiC layers and Z. Cui for his assistance with the FEM simulations. The authors also would like to thank the staff of the Else Kooi Laboratory for their support during cleanroom fabrication.

References

[1] T. Kimoto and J. A. Cooper, *Fundamentals of Silicon Carbide Technology: Growth, Characterization, Devices and Applications*. Hoboken, NJ, USA: Wiley, 2014.

[2] R. G. Azevedo *et al.*, "Silicon carbide coated MEMS strain sensor for harsh environment applications," in *Proc. IEEE 20th Int. Conf. Micro Electro Mech. Syst. (MEMS)*, Jan. 2007, pp. 643–646.

[3] N. G. Wright and A. B. Horsfall, "Sic sensors: A review," *J. Phys. D, Appl. Phys.*, vol. 40, no. 20, p. 6345, 2007. [Online]. Available: http://stacks.iop.org/0022-3727/40/i=20/a=S17

[4] D. G. Senesky, B. Jamshidi, K. Bun Cheng, and A. P. Pisano, "Harsh environment silicon carbide sensors for health and performance monitoring of aerospace systems: A review," *IEEE Sensors J.*, vol. 9, no. 11, pp. 1472–1478, Nov. 2009.

[5] L. Beker, A. Maralani, L. Lin, and A. P. Pisano, "A silicon carbide differential output pressure sensor by concentrically matched capacitance," in *Proc. IEEE 30th Int. Conf. Micro Electro Mech. Syst. (MEMS)*, Jan. 2017, pp. 981–984.

[6] S. Shao, "4h-silicon carbide pn diode for harsh environment sensing applications," Dept. Elect. Eng. Comput. Sci., Univ. California Berkeley, Berkeley, CA, USA, Tech. Rep. UCB/EECS-2016-31, May 2016. [Online]. Available: http://www.eecs.berkeley.edu/Pubs/TechRpts/2016/EECS-2016-31.html

[7] Y. Jiang, J. Li, Z. Zhou, X. Jiang, and D. Zhang, "Fabrication of all-SiC fiber-optic pressure sensors for high-temperature applications," *Sensors*, vol. 16, no. 10, p. 1660, Oct. 2016.

[8] A. C. Hoogerwerf, G. S. Durante, R. J. James, M.-A. Dubois, O. Dubochet, and M. Despont, "Silicon carbide pressure sensors for harsh environments," in *Proc. 20th Int. Conf. Solid-State Sensors, Actuat. Microsyst. Eurosensors XXXIII (TRANSDUCERS EUROSENSORS XXXIII)*, Jun. 2019, pp. 2154–2157.

[9] T.-K. Nguyen *et al.*, "Highly sensitive 4H-SiC pressure sensor at cryogenic and elevated temperatures," *Mater. Design*, vol. 156, pp. 441–445, Oct. 2018. [Online]. Available: http://www.sciencedirect.com/science/article/pii/S0264127518305458

[10] H.-P. Phan, D. V. Dao, K. Nakamura, S. Dimitrijev, and N.-T. Nguyen, "The piezoresistive effect of SiC for MEMS sensors at high temperatures: A review," *J. Microelectromech. Syst.*, vol. 24, no. 6, pp. 1663–1677, Dec. 2015.

[11] M. Eickhoff, M. Möller, G. Kroetz, and M. Stutzmann, "Piezoresistive properties of single crystalline, polycrystalline, and nanocrystalline n-type 3C-SiC," *J. Appl. Phys.*, vol. 96, no. 5, pp. 2872–2877, Sep. 2004.

[12] T. Akiyama, D. Briand, and N. F. de Rooij, "Design-dependent gauge factors of highly doped n-type 4H-SiC piezoresistors," *J. Micromech. Microeng.*, vol. 22, no. 8, Aug. 2012, Art. no. 085034. [Online]. Available: http://stacks.iop.org/0960-1317/22/i=8/a=085034

[13] G. Beheim and C. S. Salupo, "Deep RIE process for silicon carbide power electronics and MEMS," in *Proc. MRS*, vol. 622, 2011, Paper T8.9.1. [Online]. Available: https://www.cambridge.org/core/article/deep-rie-process-for-silicon-carbide-power-electronics-and-mems/65EDC46C116353B5D7D1990A1ED8413D

[14] J. Biscarrat, J. F. Michaud, E. Collard, and D. Alquier, "ICP etching of 4H-SiC substrates," *Mater. Sci. Forum*, vols. 740–742, pp. 825–828, Jan. 2013.

[15] P. Chabert, "Deep etching of silicon carbide for micromachining applications: Etch rates and etch mechanisms," *J. Vac. Sci. Technol. B, Microelectron.*, vol. 19, no. 4, pp. 1339–1345, 2001.

[16] K. M. Dowling, E. H. Ransom, and D. G. Senesky, "Profile evolution of high aspect ratio silicon carbide trenches by inductive coupled plasma etching," *J. Microelectromech. Syst.*, vol. 26, no. 1, pp. 135–142, Feb. 2017.

[17] T. Nguyen *et al.*, "Giant piezoresistive effect by optoelectronic coupling in a heterojunction," *Nature Commun.*, vol. 10, no. 1, p. 4139, Dec. 2019, doi: 10.1038/s41467-019-11965-5.

[18] T. Nguyen *et al.*, "Opto-electronic coupling in semiconductors: Towards ultrasensitive pressure sensing," *J. Mater. Chem. C*, vol. 8, no. 14, pp. 4713–4721, 2020.

[19] X. Li, F. Gao, L. Wang, L. Jiang, S. Chen, and W. Yang, "Enhanced piezoresistive performance of 3C-SiC nanowires by coupling with ultraviolet illumination," *J. Mater. Chem. C*, vol. 7, no. 43, pp. 13384–13389, 2019.

[20] L. Chen and M. Mehregany, "A silicon carbide capacitive pressure sensor for in-cylinder pressure measurement," *Sens. Actuators A, Phys.*, vols. 145–146, pp. 2–8, Jul. 2008. [Online]. Available: http://www.sciencedirect.com/science/article/pii/S0924424707007005

[21] C.-H. Wu, C. A. Zorman, and M. Mehregany, "Fabrication and testing of bulk micromachined silicon carbide piezoresistive pressure sensors for high temperature applications," *IEEE Sensors J.*, vol. 6, no. 2, pp. 316–324, Apr. 2006.

[22] H.-P. Phan *et al.*, "Robust free-standing nano-thin SiC membranes enable direct photolithography for MEMS sensing applications," *Adv. Eng. Mater.*, vol. 20, no. 1, Jan. 2018, Art. no. 1700858.

[23] V. V. Meleshko, "Bending of an elastic rectangular clamped plate: Exact versus 'engineering' solutions," *J. Elasticity*, vol. 48, no. 1, pp. 1–50, 1997, doi: 10.1023/A:1007472709175.

[24] S. P. Timoshenko and S. Woinowsky-Krieger, *Theory of Plates and Shells*. New York, NY, USA: McGraw-Hill, 1959.

[25] M. A. Fragaa, H. Furlan, M. Massia, I. C. Oliveiraa, and L. L. Koberstein, "Fabrication and characterization of a SiC/SiO_2/si piezoresistive pressure sensor," in *Proc. Eurosensors XXIV*, Linz, Austria, vol. 5, Sep. 2010, pp. 609–612. [Online]. Available: http://www.sciencedirect.com/science/article/pii/S1877705810007307

[26] K. M. Jackson, R. L. Edwards, G. F. Dirras, and W. N. Sharpe, "Mechanical properties of thin film silicon carbide," in *Proc. MRS Online Proc. Library Arch.*, vol. 687, 2001, p. B6.3.
[27] W. Zhou, J. Yang, G. Sun, X. Liu, F. Yang, and J. Li, "Fracture properties of silicon carbide thin films by bulge test of long rectangular membrane," *J. Microelectromech. Syst.*, vol. 17, no. 2, pp. 453–461, Apr. 2008.
[28] B. Morana *et al.*, "A silicon carbide MEMS microhotplate for nanomaterial characterization in TEM," in *Proc. IEEE 24th Int. Conf. Micro Electro Mech. Syst.*, 2011, pp. 380–383.
[29] K. Yasui, H. Miura, M. Takata, and T. Akahane, "SiCOI structure fabricated by catalytic chemical vapor deposition," *Thin Solid Films*, vol. 516, no. 5, pp. 644–647, Jan. 2008.
[30] J. Strass, M. Eickhoff, and G. Kroetz, "The influence of crystal quality on the piezoresistive effect of *SS*-beta/-sic between rt and 450 °c measured by using microstructures," in *Proc. Int. Solid State Sens. Actuators Conf. (Transducers)*, vol. 2, 1997, pp. 1439–1442.

Luke M. Middelburg received the B.Sc. degree in electrical engineering and the M.Sc. degree in microelectronics from the Delft University of Technology in 2014 and 2016, respectively. Previous research involves the application of impedance spectroscopy for particulate matter (PM) sensing and for the development of a fuel sensor to determine the composition of bio-ethanol containing fuel mixtures both in collaboration with Ford Motor Company, USA. Since 2016, he has been working on this Ph.D. research with the Department of Electronic Components, Technology and Materials (ECTM). Main research topics are the exploitation of non-linear effects in MEMS accelerometers and the development of silicon carbide (SiC)-based sensors. Additionally, the monolithic integration of SiC CMOS front-end read-out electronics is studied, yielding a harsh environment compatible sensing platform. This project is funded by the European Consortium Project IoSense. He is the (co)author of five journal publications, seven conference proceedings, two book chapters, and two patent applications.

H. W. van Zeijl was born in Wateringen, The Netherlands, in 1958. He studied technical physics at the Technical College, Rijswijk. He received the Diploma in Engineering degree from the Technical College in 1981 and the Ph.D. degree from the Delft University of Technology, The Netherlands, in 2005, based on research on bipolar transistors with self-aligned emitter-base metallization and back-wafer-aligned collector contacts. In 1981, he joined the Interuniversity Reactor Institute, Delft, where he worked in the field of neutron diffraction and instrumental neutron activation analysis. In 1986, he joined the Delft Institute of Microelectronics and Submicron Technology (DIMES). From 1989 to 1998, he was responsible for the mask fabrication and lithography in the DIMES IC process research sector. Since August 2017, he has been a Staff Member with the Laboratory of Electronic Components Materials and Technology (ECTM). He developed several technology courses, a full week training for engineers from relevant fields in the industry and academia. These courses are held for more than 40 times and are also given at Universities in China (Beijing, Shanghai, and Chengdu) and at companies (CNS, SHTP), Ho Chi Minh City, Vietnam. Besides these educational activities, he cooperated in different research project related to lithography, MEMs, 3-D integration, packaging, and solid state lighting integration. He is the (co) author of more than 80 technical articles and several patents.

Sten Vollebregt (Senior Member, IEEE) received the B.Sc. and M.Sc. *(cum laude)* degrees in electrical engineering from the Delft University of Technology in 2006 and 2009, respectively, and the Ph.D. degree from the Microelectronics Department, Delft University of Technology, in 2014, on the low-temperature high-density growth of carbon nanotubes for application as vertical interconnects in 3-D monolithic integrated circuits. For his master thesis, he investigated the growth of carbon nanotubes at the NanoLab, Newton, MA, USA, and AIXTRON, Cambridge, U.K. After obtaining his Ph.D., he held a postdoctoral position on the wafer-scale integration of graphene for sensing applications together with the Faculty of Mechanical Engineering and several industrial partners. During this research, he developed a unique transfer-free wafer-scale CVD graphene process. Since October 2017, he has been an Assistant Professor with the Laboratory of Electronic Components, Technology and Materials, Delft University of Technology, where his research focuses on the integration of emerging electronic materials into semiconductor technology for sensing applications. His research interests include (carbon-based) nanomaterials, 3-D monolithic integration, wide-bandgap semiconductors, and (harsh) environmental sensors. He has coauthored over 25 journal publications, four book chapters, and holds three patents.

Bruno Morana received the M.Sc. degree in electronic engineering from the Politecnico di Milan, Milan, Italy, in 2007. He is currently pursuing the Ph.D. degree with the Laboratory of Electronic Components Technology and Materials, with a focus on the fabrication of surface micromachined nanoreactors made of silicon carbide. During the master's thesis, he joined the Electronic Technology Department, Polytechnic University of Madrid, Madrid, Spain, where he was a Researcher. His master's thesis and research activity focused on the fabrication and characterization of Si and SiGe nanocrystals embedded in SiO_2 thin films. In 2008, he joined the Laboratory of Electronic Components Technology and Materials, Delft University of Technology, Delft, The Netherlands, as a Researcher. He focused on the development and optimization of procedures for the ultrahigh vacuum compatible assembly of MEMS nanoreactors. His research interests include the fabrication and characterization of thin films and the development of fabrication technologies for MEMS devices.

Guoqi Zhang (Fellow, IEEE) received the Ph.D. degree from the Delft University of Technology, The Netherlands, in 1993. He is a Chair Professor of Micro/Nanoelectronics System Integration and Reliability with the Delft University of Technology. His research interests include multilevel heterogeneous system integration and packaging, wide band gap semiconductors sensors and components, multiphysics and multiscale modeling of micro/nanoelectronics, and digital twin for mission critical multifunctional electronics components and systems. He has authored/coauthored more than 400 scientific publications. He serves as the Deputy Director of the European Center for Micro- and Nanoreliability (EUCEMAN), the Co-Chair of the Advisory Board of International Solid State Lighting Alliance (ISA), and the Secretary General of the International Technology Roadmap of Wide Bandgap Semiconductors (ITRW). He has worked for NXP Semiconductors as the Senior Director of Technology Strategy until 2009 and a Philips Research Fellow until May 2013.